

## PDF hosted at the Radboud Repository of the Radboud University Nijmegen

The following full text is a publisher's version.

For additional information about this publication click this link.

<http://hdl.handle.net/2066/75351>

Please be advised that this information was generated on 2017-12-06 and may be subject to change.

## Competing anisotropies in bcc Fe<sub>81</sub>Ni<sub>19</sub>/Co(001) superlattices

H. Hafermann,<sup>1,a)</sup> R. Bručas,<sup>2</sup> I. L. Soroka,<sup>3</sup> M. I. Katsnelson,<sup>4</sup> D. Iušan,<sup>2</sup> B. Sanyal,<sup>2</sup> O. Eriksson,<sup>2</sup> and B. Hjörvarsson<sup>2</sup>

<sup>1</sup>*Institute of Theoretical Physics, University of Hamburg, 20355 Hamburg, Germany*

<sup>2</sup>*Department of Physics and Materials Science, Uppsala University, P.O. Box 530, 751 21 Uppsala, Sweden*

<sup>3</sup>*Department of Materials Chemistry, Uppsala University, P.O. Box 576, 751 23 Uppsala, Sweden*

<sup>4</sup>*Institute for Molecules and Materials, Radboud University, 6525 AJ Nijmegen, The Netherlands*

(Received 9 November 2008; accepted 23 January 2009; published online 17 February 2009)

A magnetization reorientation transition has been observed in Fe<sub>81</sub>Ni<sub>19</sub>/Co(001) superlattices by means of magneto-optical Kerr effect and magnetic force microscopy measurements. The transition is driven by the variation of the interface density. First-principles calculations are combined with a linear stability analysis of the Landau–Lifshitz equation to clarify the mechanism that drives the transition. We are able to identify it as being driven by competing interface in-plane and uniaxial bulk out-of-plane anisotropies. The origin of the bulk anisotropy is attributed to tetragonal distortions experimentally observed in these superlattices. © 2009 American Institute of Physics. [DOI: 10.1063/1.3081107]

Tailoring magnetic anisotropies is vital for technological applications such as magnetic recording. While the use of multilayered composite magnetic structures provides additional degrees of freedom for tuning the magnetic properties, their understanding is complicated as bulk and interface anisotropies and interlayer exchange properties must be taken into account.<sup>1</sup> It is well known that the reduced symmetry caused by lattice distortions can give rise to a strong enhancement of the magnetic anisotropy energy (MAE).<sup>2</sup> A strong MAE enhancement has been found by reducing the symmetry in creating Fe/Co superlattices.<sup>3</sup> Interface anisotropies have been previously reported in Co based systems.<sup>4,5</sup>

In this letter, we report on a spin-reorientation transition observed in Fe<sub>81</sub>Ni<sub>19</sub>/Co superlattices by variation of the interface density. The combination of *ab initio* calculations with the Landau–Lifshitz equation (LLE) allows us to elucidate the origin and unravel the interplay of the magnetic anisotropies in these superlattices. Our results show that the uniaxial bulk anisotropy contribution is indeed as large as expected from *ab initio* calculations and originates from tetragonal distortions of the layers. The effective anisotropy however is substantially reduced due to a competing in-plane anisotropy originating from the FeNi/Co interface.

The superlattices have been prepared by dc-magnetron sputtering on single crystal MgO(001) substrates at 170 °C. Deposition rates controlled by quartz microbalance of 0.035 and 0.08 nm/s for FeNi and Co, respectively, were calibrated against thickness measurements using low angle x-ray diffraction. The superlattices contain repetitions of bilayers (BLs) with the same number of monolayers for FeNi and Co. The thickness of the individual layers was varied in the range of 1–12 ML which ensures the same bcc phase in all superlattices. The total thickness was kept constant at 350 ± 5 nm, while varying the number of BLs from 1200 down to 100. Hence the interface density was varied while keeping the composition and ratio of the constituents constant. Care was taken in maintaining the same growth conditions for all

samples to ensure the same quality of the interfaces. In Fig. 1 we show the X-ray reflectivity data together with the simulation. The presence of superlattice peaks up to the fifth order indicates a distinct compositional modulation along the growth direction. From the simulation we have determined a typical layer thickness variation (referred to as roughness) of 1.5 ± 0.3 ML for all samples with individual layer thickness larger than a monolayer. Indeed, the presence of a first order superlattice peak in the sample consisting of repetitions of 2 ML FeNi and 2 ML Co (2/2 ML) indicates the roughness to be below 2ML. The measured structural and magnetic properties of the 1/1 ML sample showed no different features from a sample prepared by codeposition of FeNi and Co, so that we consider it to be a bcc FeNi–Co alloy film.

The magnetic properties of the superlattices were studied by magneto-optical Kerr effect (MOKE) and magnetic force microscopy (MFM) measurements. MOKE hysteresis loops measured along the [110] direction for different samples are shown in Fig. 2. The 8/8 ML (150BL) sample (a) is magnetized in the plane. A weak cubic anisotropy<sup>6</sup> stabilizes the magnetization along [110] and prevents in-plane rotation. Hence, for the 9/9 ML (133BL) sample (b), an in-plane remanence less than one indicates the magnetization being slightly tilted out of the plane. This is more clearly seen when increasing the individual layer thickness to 10 ML

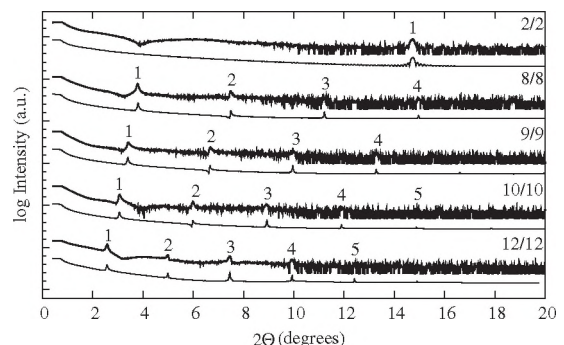


FIG. 1. X-ray reflectivity scans (thick lines) together with corresponding simulated data (thin lines). Superlattice peaks are found for all samples with individual layer thicknesses down to 2 ML (2/2).

<sup>a)</sup>Electronic mail: hartmut.hafermann@physnet.uni-hamburg.de.



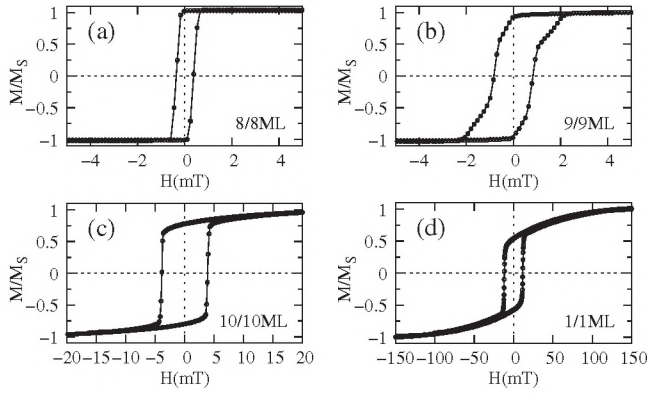


FIG. 2. In-plane hysteresis loops obtained from magneto-optical Kerr effect measurements for different samples measured along [110]: (a) 8/8 ML, (b) 9/9 ML, and (c) 10/10 ML. The SRT is revealed by a decreasing remanence when the layer thickness is increased. Samples with layer thickness below 8 ML are magnetized in the plane, except for the 1/1 ML sample shown in (d), which exhibits out-of-plane magnetization.

(100BL) in sample (c). The presence of domains is confirmed by the MFM measurements as discussed below. Hence the MOKE measurements reveal a spin reorientation transition (SRT) from a homogeneously in-plane magnetized state to a state with out-of-plane magnetization as the interface density is reduced. While the samples from 2/2 ML to 8/8 ML were found to be magnetized in the plane, the 1/1 ML sample (d) again exhibits out-of-plane magnetization and a stripe domain structure.

For the superlattices it has been established that the layers are tetragonally distorted.<sup>7</sup> The  $\text{Fe}_{81}\text{Ni}_{19}$  layers are expanded along the  $c$ -axis ( $c=2.89$  Å), while the Co layers are compressed with  $c=2.82$  Å, compared to the in-plane lattice parameters  $a=b=2.84$  Å. This tetragonal distortion is expected to give rise to a rather large uniaxial anisotropy. Indeed, by extrapolating the *ab initio* data in Ref. 2, according to the measured distortions, yields a perpendicular anisotropy energy  $E_a=K_u(M_z/M_s)^2$  with  $K_u=-4.182 \times 10^5$  J/m<sup>3</sup> for FeNi and  $-0.899 \times 10^5$  J/m<sup>3</sup> for Co. Notably both anisotropies have the same sign corresponding to a perpendicular easy axis.

In order to elucidate the mechanism that drives the transition, we have developed a realistic description of the superlattices. Close to the SRT this is achieved by solving a linearized LLE with the parameters obtained either from first-principles calculations or experimental data. We assume the superlattices to be infinitely extended in the  $x$ - $y$ -plane. In the vicinity of the SRT the magnetization is mainly aligned along the  $y$ -direction and written as  $\mathbf{M}=M_s(m_x, 1+m_y, m_z)$  with  $m_{x,z} \ll 1$  and  $m_y \approx -1/2(m_x^2+m_z^2) \approx 0$ . Inserting this into the LLE

$$\frac{1}{\gamma} \frac{\partial \mathbf{M}}{\partial t} = \mathbf{M} \times \mathbf{H}^{\text{eff}} \quad (1)$$

( $\gamma$  is the gyromagnetic ratio) and neglecting all terms quadratic in the small perpendicular components  $m_x$  and  $m_z$  yields two linear equations for  $m_{x,z}$ . In order to account for the shape anisotropy, these equations should be supplemented by Maxwell's equations for the demagnetizing field  $\mathbf{H}^d$ :  $\nabla \times \mathbf{H}^d = 0$  and  $\nabla \cdot (\mathbf{H}^d + \mathbf{M}) = 0$ . This is equivalent to a single equation  $\nabla \cdot \mathbf{M} - \Delta \phi = 0$  for the magnetic potential  $\phi$  defined by  $\mathbf{H}^d = -\nabla \phi$ . Since we solve a linear equation, we

may represent the solution in the form of  $m_{x,z}(x, z, t) = m_{x,z}(\kappa, k, \Omega) \exp[i(\kappa x + kz + \Omega t)]$  and similar for  $\phi$  ( $\Omega$ ,  $\kappa$ , and  $k$  are normalized frequency and wave vectors, respectively, and time and space coordinates have been rescaled). The general solution is obtained by linear superposition. Inserting this into the LLE yields a linear system for the Fourier components  $m_{x,z}(\kappa, k, \Omega)$ . For given  $\kappa$  and  $\Omega$ , only certain  $k$ -values are allowed. The solution within each layer is a superposition of the solutions for the allowed values of  $k$ . We have to match these at the interfaces and surfaces using certain boundary conditions. For example, the Hoffmann boundary conditions<sup>8</sup> account for the interface anisotropy ( $E_{\text{int}}$ ) and interface exchange contributions ( $A_{\text{int}}$ ),

$$\mathbf{M}_l \times \left( \nabla_{\mathbf{M}_l} E_{\text{int}}[\mathbf{M}] - \frac{2A_l}{M_l^2} \frac{\partial \mathbf{M}_l}{\partial n_l} - \frac{2A_{\text{int}}}{M_l M_{l'}} \mathbf{M}_{l'} \right) \Bigg|_{z=z_l} = 0$$

(there is a second condition with layer indices  $l$  and  $l'=l+1$  exchanged). Maxwell's equations provide an additional boundary condition. For a given wave vector  $\kappa$ , the solubility condition, that the determinant of the boundary condition matrix be zero, defines the spin wave dispersion of the superlattice  $\Omega^2(\kappa)$ . For further details we refer the interested reader to Ref. 6. We use exchange constants  $A_{\text{FeNi}}=1.596 \times 10^{-11}$  and  $2.173 \times 10^{-11}$  J/m for Co which enter through the effective field  $\mathbf{H}^{\text{eff}}(\mathbf{r}, t) = (2A/M^2)\Delta \mathbf{M} - \nabla_{\mathbf{M}} E_a + \mathbf{H}^d$  in Eq. (1). The interface exchange constant has been determined for an independent set of samples<sup>6</sup> to be  $A_{\text{int}} \approx 30 \times 10^{-3}$  J/m<sup>2</sup>, which reveals a strong coupling between FeNi and Co. In the same calculation we find that in order to achieve agreement with the experiment, it is necessary to introduce an interface anisotropy of  $K_i=0.273 \times 10^{-3}$  J/m<sup>2</sup>. This has the same order of magnitude as the one given in Ref. 4 for the Co/Pd system, albeit with opposite sign.

In Fig. 3, we show spin wave dispersions  $\Omega^2(\kappa)$  obtained from the LLE together with the corresponding MFM images. For the 8/8 ML sample, the solution with lowest energy (frequency) occurs at  $\kappa=0$ , corresponding to homogeneous in-plane magnetization. The spin waves with higher energy correspond to oscillations around the stable in-plane magnetization  $m_{x,z} \sim \exp(i\Omega t)$ . For the 9/9 ML sample, solutions with imaginary frequency ( $\Omega^2 < 0$ ) exist in the dispersion which grow exponentially in time, i.e.,  $m_{x,z} \sim \exp(|\Omega|t)$ . These are unbounded because damping was not taken into account. The presence of these solutions implies that the assumed in-plane magnetization is unstable, in agreement with the appearance of a domain structure in the MFM image. The stripes form along [110], the direction of the previously applied field. This direction was chosen to coincide with that of the aforementioned cubic anisotropy, which stabilizes the stripe direction. The unique wave vector  $\kappa_0$  for which the solutions grow fastest (at the minimum of the dispersion) determines the period of the domain structure in the sample. Close to the transition a segmented stripe domain structure appears at the expense of the formation of additional domain walls<sup>9</sup> as seen in the MFM image for the 9/9 ML sample. A quantitative two-dimensional Fourier-transform analysis yields a width of  $400 \pm 45$  nm (perpendicular to the magnetization direction) and a length of  $500 \pm 55$  nm of the stripe segments on average. The large error bar is due to the irregularity of the domain structure close to the transition.



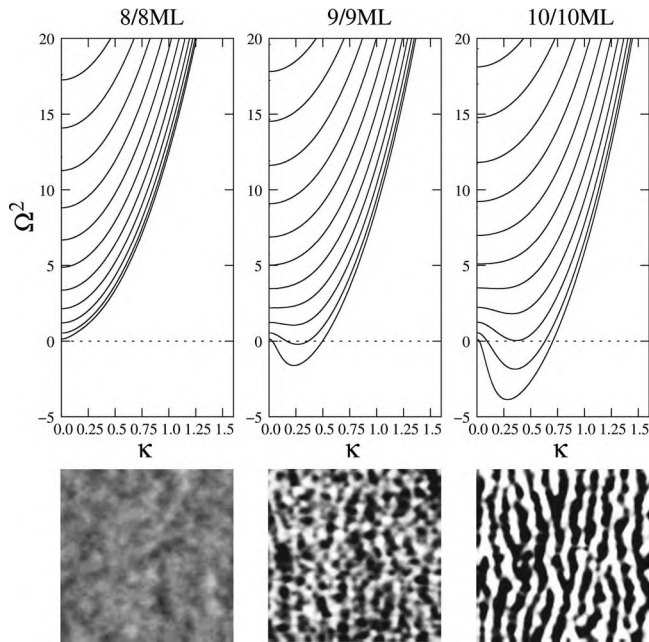


FIG. 3. Spin wave dispersion for the 8/8, 9/9, and 10/10 ML samples in zero external field together with the respective MFM images (scan area of  $5 \times 5 \mu\text{m}$ ).  $\kappa$  and  $\Omega$  are normalized wave vector and frequency, respectively. Branches with  $\Omega^2 < 0$  signal the departure from the homogeneously magnetized in-plane single-domain state and the presence of a domain structure in the sample. The range in  $\kappa$  corresponds to a range of  $1.01 \times 10^6 \text{ cm}^{-1}$  and the frequency range is approximately 16 GHz.

The formation of segmented stripe domains is not considered in the calculation since we assumed the sample to be homogeneously magnetized along the stripe direction. However, from the wave vector  $\kappa_0$  we find a domain period of 405 nm, which agrees remarkably well with the experimental value of 400 nm. For the 10/10ML sample the domain wall contribution of the Néel walls is more significant as the magnetization is tilted further out of plane and hence the formation of these walls is suppressed leading to formation of more regular stripes. A comparison of the domain period of this sample to its theoretical value, however, is not possible since the linearized equation does not provide a reliable estimate away from the transition.

The interface anisotropies are of the same order of magnitude as the bulk anisotropy close to the transition. For the 9/9ML sample, the effective volume contribution due to the interfaces is  $K_{\text{eff}} = 2.12 \times 10^5 \text{ J/m}^3$ , which competes with an average bulk anisotropy of  $\bar{K}_u = -2.56 \times 10^5 \text{ J/m}^3$ . The ef-

fective anisotropy of  $K_{\text{eff}} = 2.39 \times 10^5 \text{ J/m}^3$  in the 8/8 ML sample even cannot compensate the bulk anisotropy by itself. Here the additional effect of the shape anisotropy stabilizes the in-plane magnetization.

To conclude, we have observed a SRT in the  $\text{Fe}_{81}\text{Ni}_{19}/\text{Co}$  superlattices, which is very well described by the solution of a linearized LLE with parameters obtained from the *ab initio* calculations and experimental data. The transition is driven by the competition between the bulk magnetocrystalline and interface anisotropies, the latter originating from the  $\text{Fe}_{81}\text{Ni}_{19}/\text{Co}$  interface. The results lead us to conclude that tetragonal distortions are the source of the perpendicular anisotropy in these samples. A change in the bulk anisotropy by varying the layer thickness may be ruled out as essentially the same out-of-plane lattice parameter was measured for 4/4, 8/8 and 12/12 ML samples.<sup>7</sup> Since the interface anisotropy is responsible for the homogeneous in-plane single domain states, the reappearance of the domain structure in the 1/1 ML sample is naturally explained by the absence of the  $\text{FeNi}/\text{Co}$  interface. Our results imply that the magnetization direction of a specimen can be tuned in a controlled way while leaving other properties such as density, composition, hardness and softness, shape, and thickness unaffected. This may be important, e.g., for magnetic data storage applications.

Financial support from the DFG Grant No. SFB 668 (Germany), the Swedish Research Council (VR), the Swedish Foundation for Strategic Research (SSF), and the Göran Gustafsson foundation are acknowledged.

<sup>1</sup>A. P. Popov, N. V. Skorodumova, and O. Eriksson, *Phys. Rev. B* **77**, 014415 (2008).

<sup>2</sup>T. Burkert, O. Eriksson, P. James, S. I. Simak, B. Johansson, and L. Nordström, *Phys. Rev. B* **69**, 104426 (2004).

<sup>3</sup>V. A. Vas'ko, M. Kim, O. Mryasov, V. Sapozhnikov, M. K. Minor, A. J. Freeman, and M. T. Kief, *Appl. Phys. Lett.* **89**, 092502 (2006).

<sup>4</sup>B. N. Engel, C. D. England, R. A. Van Leeuwen, M. H. Wiedmann, and C. M. Falco, *Phys. Rev. Lett.* **67**, 1910 (1991).

<sup>5</sup>L. F. Schelp, G. Tosin, M. Carara, M. N. Baibich, A. A. Gomes, and J. E. Schmidt, *Appl. Phys. Lett.* **61**, 1858 (1992).

<sup>6</sup>R. Brucas, H. Hafermann, I. L. Soroka, D. Iuşan, B. Sanyal, M. I. Katsnelson, O. Eriksson, and B. Hjörvarsson, *Phys. Rev. B* **78**, 024421 (2008).

<sup>7</sup>I. L. Soroka, R. Brucas, V. Stanciu, P. Nordblad, and B. Hjörvarsson, *J. Magn. Magn. Mater.* **277**, 228 (2004).

<sup>8</sup>F. Hoffmann, A. Stankoff, and H. Pascard, *J. Appl. Phys.* **41**, 1022 (1970).

<sup>9</sup>R. Brucas, H. Hafermann, M. I. Katsnelson, I. L. Soroka, O. Eriksson, and B. Hjörvarsson, *Phys. Rev. B* **69**, 064411 (2004).